NANO LETTERS
Letter
pubs.acs.org/NanoLett

Monitoring Local Strain Vector in Atomic-Layered $MoSe_2$ by Second-Harmonic Generation

Jing Liang,[†] Jin Zhang,[‡] Zhenzhu Li,[§] Hao Hong,[†] Jinhuan Wang,[†] Zhihong Zhang,[†] Xu Zhou,[†] Ruixi Qiao,[†] Jiyu Xu,[‡] Peng Gao,[†] Zhirong Liu,[§] Zhongfan Liu,[§] Zhipei Sun,[*,∥] Sheng Meng,[*,‡] Kaihui Liu,[*,†] and Dapeng Yu[†,⊥]

[†]State Key Laboratory for Mesoscopic Physics, Collaborative Innovation Center of Quantum Matter, School of Physics, Academy for Advanced Interdisciplinary Studies, Peking University, Beijing 100871, China

[‡]Beijing National Laboratory for Condensed Matter Physics, and Institute of Physics, Chinese Academy of Sciences, Beijing 100190, China

[§]Centre for Nanochemistry, College of Chemistry and Molecular Engineering, Peking University, Beijing 100871, China

[∥]Department of Electronics and Nanoengineering, Aalto University, Espoo 02150, Finland

[⊥]Department of Physics, Southern University of Science and Technology, Shenzhen 518055, China

S *Supporting Information*

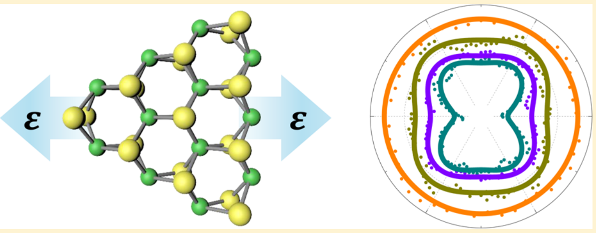

ABSTRACT: Strain serves as a powerful freedom to effectively, reversibly, and continuously engineer the physical and chemical properties of two-dimensional (2D) materials, such as bandgap, phase diagram, and reaction activity. Although there is a high demand for full characterization of the strain vector at local points, it is still very challenging to measure the local strain amplitude and its direction. Here, we report a novel approach to monitor the local strain vector in 2D molybdenum diselenide ($MoSe_2$) by polarization-dependent optical second-harmonic generation (SHG). The strain amplitude can be evaluated from the SHG intensity in a sensitive way (−49% relative change per 1% strain); while the strain direction can be directly indicated by the evolution of polarization-dependent SHG pattern. In addition, we employ this technique to investigate the interlayer locking effect in 2H $MoSe_2$ bilayers when the bottom layer is under stretching but the top layer is free. Our observation, combined with ab initio calculations, demonstrates that the noncovalent interlayer interaction in 2H $MoSe_2$ bilayers is strong enough to transfer the strain of at least 1.4% between the bottom and top layers to prevent interlayer sliding. Our results establish that SHG is an effective approach for in situ, sensitive, and noninvasive measurement of local strain vector in noncentrosymmetric 2D materials.

KEYWORDS: *strain, $MoSe_2$, second-harmonic generation, 2D materials*

Since the discovery of graphene, two-dimensional (2D) materials such as transition metal dichalcogenides (TMDCs), black phosphorus, hexagonal boron nitride (h-BN), and other compounds have received extensive attention due to their fascinating physical properties and potential applications.[1−15] For flexible device design using 2D materials, it is of significant importance to engineer their properties in a controllable way. Currently, strain engineering represents a very efficient and powerful route for this purpose, benefiting from the ultraflexibility and ultratoughness of 2D materials.[16−23] Accordingly, the development of suitable techniques to precisely characterize both the amplitude and direction of the local strain vector is a prerequisite for future applications. Conventionally in electron/neutron microscopy,[24,25] photoluminescence (PL) spectroscopy, or Raman spectroscopy,[26,27] the strain vector information is typically obtained by mapping out all the strain amplitude in a 2D plane point by point. However, it is impossible to measure the in-plane strain direction with these approaches (for example, the sample size is comparable with the probing beam spot); and only in special cases when materials have a doubly degenerate in-plane phonon mode that can split under uniaxial strain, it is possible to indicate the strain direction by polarization-dependent Raman spectroscopy.[28−30] Nevertheless, there is a great demand for the development of effective techniques to monitor the local strain vector with high resolution.

Recently, optical second-harmonic generation (SHG) microscopy/spectroscopy has been developed to probe the crystallographic orientation, grain boundaries, and stacking order of noncentrosymmetric 2D materials, such as TMDCs, h-BN, and GaSe.[31−39] As the optical field of the SHG is proportional to the nonlinear optical susceptibility, the SHG intensity is very sensitive to the structural configurations of 2D

Received: August 14, 2017
Revised: November 19, 2017
Published: November 22, 2017

DOI: 10.1021/acs.nanolett.7b03476
Nano Lett. 2017, 17, 7539−7543

materials. In principle, it is plausible to utilize SHG to monitor the strain in 2D materials, as strain will change the lattice structure and thus the optical susceptibility of the material. In this letter, for the first time, we utilize the polarization-dependent SHG technique to monitor the local strain vector in atomic-layer molybdenum diselenide ($MoSe_2$). Our results demonstrate that this technique can in situ sensitively and noninvasively probe both the strain amplitude and direction in monolayer $MoSe_2$ only with a single-point measurement. We further apply this technique to investigate the interlayer locking effect in 2H $MoSe_2$ bilayer and find that at least 1.4% strain could be transferred from the bottom layer to the top layer.

In our experiment, triangle-shaped monolayer or bilayer $MoSe_2$ flakes were grown by chemical vapor deposition (Figure 1a, see Supporting Information (SI) for details). The layer number of $MoSe_2$ flakes can be identified by optical contrast and Raman spectroscopy.[40,41] Both the monolayer and bilayer samples have A_{1g} and E^1_{2g} modes, but the bilayer (with 2H stacking) has a characteristic shearing C mode in the Raman spectra (Figure 1b). We transferred $MoSe_2$ flakes on an optical transparent acrylic substrate using poly(methyl methacrylate) (PMMA) method or directly grew (exfoliated) $MoSe_2$ on a mica substrate (see SI for details). Uniaxial tensile strain is applied on the $MoSe_2$ flakes by bending the flexible acrylic (mica) substrates.[21] As the acrylic (mica) substrate has relative large Young's modulus and can transfer the strain from itself to the 2D materials very effectively,[22] one can simply calculate the applied strain amplitude from the curving geometry of the substrate by $\varepsilon = \tau/2\rho$, where τ is the thickness of the substrate and ρ is the curvature radius of the neutral plane (Figure 1c). We first check if the strain is indeed effectively applied to monolayer $MoSe_2$ by monitoring the evolution of the PL peak energy. As the strain increases, the PL peak linearly shifts to lower energy. The slope is determined to be −36.8 meV/ε, and the relative change slope ($\frac{\Delta E_\varepsilon}{E_0} = \frac{E_\varepsilon - E_0}{E_0}$, where E_ε and E_0 stand for the PL peak energy with and without strain, respectively) is −0.023/ε (Figure 1d and Figure S1). The slope is consistent with the previous experiments of $MoSe_2$, and therefore, the strain amplitude can be calculated from the geometric shape of the bent substrate[23] and the PL peak energy shift. In all studies below, we use both approaches to obtain the strain amplitude. Note that all optical measurements are taken near the center of the monolayer $MoSe_2$ triangles to ensure the position correspondence between different techniques (Figure S2).

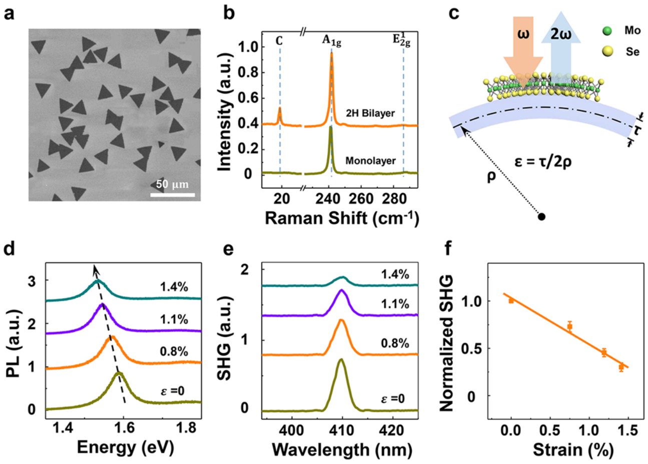

Figure 1. PL and SHG response to strain in monolayer $MoSe_2$. (a) SEM images of CVD-grown monolayer $MoSe_2$ triangles. (b) Raman spectroscopy of monolayer and bilayer $MoSe_2$. (c) Schematic of strain apparatus and SHG process in monolayer $MoSe_2$ under uniaxial tensile strain. The left orange and right blue arrows indicate excitation beam (ω) and generated SHG signal (2ω), respectively. (d) PL spectra of monolayer $MoSe_2$ under different strain amplitudes. The dash arrow indicates the redshift direction of PL peaks, with a slope of −36.8 meV/ε. (e) SHG spectra under different strain. (f) Evolution of normalized SHG intensity with strain. Line is the linear fit to the experimental data. The error bars represent the standard measurement error from experiments of 12 samples.

We then investigate the strain-dependent SHG intensity. As monolayer $MoSe_2$ belongs to the noncentrosymmetric D_{3h} point group, it allows appreciable second-order nonlinear optical response.[31−38] Under excitation of linearly polarized femtosecond pulses (wavelength of 820 nm, pulse width of ~100 fs), the intensity of reflected SHG signal centering at 410 nm changes under different strain amplitudes (Figure 1e). It clearly indicates that the SHG intensity is very sensitive to the strain. Detailed analysis (Figure 1f) shows that the relative change in SHG intensity ($\frac{\Delta I_\varepsilon}{I_0} = \frac{I_\varepsilon - I_0}{I_0}$, where I_ε and I_0 stand for SHG intensity with and without strain, respectively) is linearly related to the strain amplitude. The slope is determined to be −0.49 ± 0.05/ε, which is one order of magnitude larger than the relative change of PL peak energy. Such relatively large linear relation facilitates the monitoring of the strain amplitude directly and sensitively by the SHG intensity. Although theoretically it is of great challenge to quantitatively predict the SHG intensity under strain by first-principles calculations,[42] in practice we demonstrate that SHG is a very effective technique to characterize the strain amplitude.

In order to monitor the strain direction, we change the polarization direction of the excitation laser to investigate the polarization-dependent SHG intensity pattern. If the polarization of the output SHG signal is parallel ($I_\parallel$) or perpendicular ($I_\perp$) to that of the excitation laser, the SHG intensity in $MoSe_2$ exhibits 6-fold rotational symmetry: $I_\parallel = I\cos^2(3\theta)$, $I_\perp = I\sin^2(3\theta)$, where θ is the angle between the excitation laser polarization and crystalline armchair direction of monolayer $MoSe_2$[31−34] and the total SHG intensity, $I = I_\perp + I_\parallel$, is independent of θ. In our SHG measurement, $\theta = \theta' + \theta_0$, where θ' is the angle between laser polarization and horizontal direction (the uniaxial tensile strain is applied to) as shown in Figure 2a, and θ_0 is the angle between horizontal and crystalline armchair direction. The laser polarization is controlled by rotating a half-wave plate before the objective, while the SHG signal is analyzed by a polarizer in front of the detector. Therefore, from the θ'-dependent SHG pattern of $I_\parallel$, the microscopic armchair crystalline orientation θ_0 can be identified from the direction of six petals (Figure 2b,f), which has a clear correlation to the macroscopic triangle shape of monolayer $MoSe_2$ as shown in Figure 2a,e. Furthermore, we choose $MoSe_2$ triangles of different orientations to the strain direction (ε_z or ε_a represents the two high symmetric cases when the strain is along the crystalline armchair or the zigzag direction of $MoSe_2$). Figure 2b−d (f−h) shows the pattern evolution of $I_\parallel$, $I_\perp$, and I when strain ε_a (ε_z) is applied to monolayer $MoSe_2$. Without strain, $I_\parallel$ and $I_\perp$ with six petals of the same size reveal three-fold rotation symmetry of the 2D crystal, and the total SHG intensity I has a circular shape. Once the strain is applied, the SHG pattern distorts significantly. The SHG intensity decreases

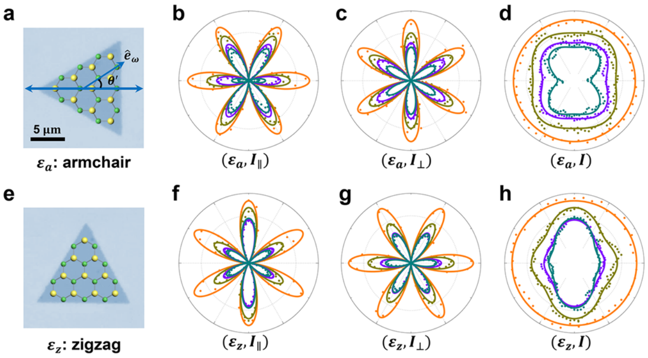

Figure 2. Pattern evolution of SHG intensity for monolayer $MoSe_2$ under strain. (a) Optical image of monolayer $MoSe_2$ under strain ε_a along the crystalline armchair direction. The strain is along the horizontal direction indicated by a double-headed arrow, while the laser excitation polarization $\hat{e}_\omega$ has a relative angle θ' to it. The ball and stick model shows the crystalline structure. (b−d) θ'-dependent SHG intensity pattern when the polarization of generated SHG is parallel (b), perpendicular (c) to the incident polarization, or the total SHG (d) under strain ε_a. (e−h) The counterpart data under strain ε_z along the crystalline zigzag direction. The laser polarization, strain direction, and image size are the same as shown in (a). Dots are original data and lines are theoretical fits; while the colors of orange, dark yellow, violet, and dark cyan (from outer curves to inner ones) represent strain amplitude of 0, 0.8%, 1.14%, and 1.4% in sequence for (b−d, f−h).

rapidly with increasing strain in each petal, and the $I_\parallel$ or $I_\perp$ shape of the six petals become asymmetric, and the total SHG intensity I shows up a strong angular dependence. The strain direction could be indicated by the minor axis of the pattern of I. Additionally, the pattern modes of I are different for different strain orientations. The I pattern looks like a dumbbell with ε_a (Figure 2d), while the pattern seems as a spindle with ε_z (Figure 2h). For another strain direction ε_c (i.e., the strain is not along zigzag or armchair crystalline direction of $MoSe_2$), the results are more complex (see Supplementary Figure S3). Nevertheless, the strain direction can also be easily deduced from the SHG pattern evolution. For other noncentrosymmetric 2D materials such as monolayer MoS_2, we also observe similar SHG pattern evolution with a strain induced SHG change ratio of $\sim -0.37/\varepsilon$ (Supplementary Figures S4 and S5). This indicates that our method should be generally applicable to noncentrosymmetric 2D materials.

To qualitatively understand the SHG pattern evolution under uniaxial tensile strain, we consider the nonlinear SHG response in terms of point group symmetry. The polarization-dependent SHG intensity could be expressed as

$$I_{SHG} = |\hat{e}_{2\omega} \overleftrightarrow{d} \hat{e}_\omega{}^2|^2 \tag{1}$$

where $\hat{e}_{2\omega}$ and $\hat{e}_\omega$ are, respectively, the polarization orientation of generated SHG electric field and incident electric field, and $\overleftrightarrow{d}$ is contracted notation of second-order susceptibility tensor, which is a 3 × 6 matrix.[43] Under uniaxial strain, the matrix of $\overleftrightarrow{d}$ evolves from the three-fold D_{3h} symmetry into C_{2v} symmetry, which is the origin for the observed SHG pattern evolution in Figure 2. As the number and relative magnitude of independent nonzero matrix elements of $\overleftrightarrow{d}$ are different for different θ' angles, the SHG pattern evolution can reflect the strain direction.

We can further quantitatively evaluate the SHG pattern evolution for the two highly symmetric cases by analytical equations based on first-order perturbation. On the basis of normal incidence geometry, the effective elements in $\overleftrightarrow{d}^{(C_{2v})}$ aligned into D_{3h} coordinate have the same form as $\overleftrightarrow{d}^{(D_{3h})}$. It is supposed that $d_{il}^{(C_{2v})}$ varies linearly with small external strain perturbation (see SI for detail). Then, the polarization-dependent SHG intensity of monolayer $MoSe_2$ under ε_a behaves as follows:

$$\begin{aligned} I_\parallel^{(C_{2v})} &= |d_{22}^{(D_{3h})}(\cos 3\theta + \varepsilon_a(a_1 \cos^3\theta - b_1 \sin^3\theta \cos\theta \\ &\quad - 2c_1 \sin^3\theta \cos\theta))|^2 \\ I_\perp^{(C_{2v})} &= |d_{22}^{(D_{3h})}(\sin 3\theta + \varepsilon_a(a_1 \sin\theta \cos^2\theta - b_1 \sin^3\theta \\ &\quad + 2c_1 \sin\theta \cos^2\theta))|^2 \end{aligned} \tag{2}$$

where a_1, b_1, and c_1 are the relative changes of different tensor elements in $\overleftrightarrow{d}$ caused by strain perturbation. Under ε_z, we would obtain the same formula as shown above with parameters of ε_z, a_2, b_2, and c_2. The total SHG intensity $I^{(C_{2v})}$ is the sum of $I_\parallel^{(C_{2v})}$ and $I_\perp^{(C_{2v})}$. With this analytic model, we can reproduce our experimental data and extract the fitting parameters for a_i, b_i, and c_i (see Supplementary Figure S6 and Table S1). When the strain is along the high symmetric ε_z and ε_a direction, both the minor axis and the shape of I can indicate the strain direction (Figure 2d,h). For a general case when the strain is along nonarmchair/zigzag direction, the strain direction can also be obtained from the SHG pattern evolution (Supplementary Figure S3), although the analytical equation is more complex (see SI for detail). Here, we note that the quantitative ab initio theories for understanding the pattern evolution is still lacking. Our results might evoke the further development of theory in this direction in the future.

As SHG is a very sensitive and effective way to monitor the local strain in $MoSe_2$ monolayer, we further employ it to investigate the interlayer locking effect between the two layers in AB-stacked (2H) $MoSe_2$ bilayer when the bottom layer is under stretching but the top layer is free (Figure 3a). Bulk $MoSe_2$ is believed to be a lubricant as MoS_2 and the interlayer sliding should be quite easy.[44−46] Whether the interlayer interaction can lock the two layers under relative interlayer strain and if so how large the relative strain can be locked are still under debate. Furthermore, this information is also crucial for evaluating the performance and mechanical stability of van der Waals stacked multilayer 2D flexible devices under strain.

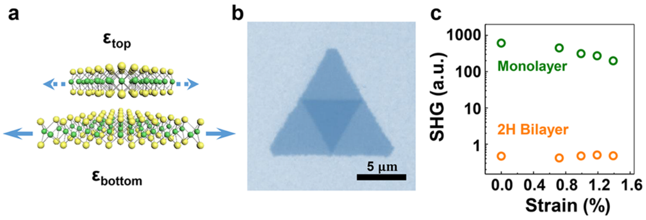

Figure 3. Monitoring the interlayer locking behavior in 2H bilayer $MoSe_2$. (a) Schematic diagram of 2H $MoSe_2$ bilayer when the bottom layer is under stretching but the top layer is free. ε_{bottom} is directly applied to the bottom layer from the bending substrate; ε_{top} is the possible strain on the top layer that can be transferred from the bottom layer. (b) Optical image of 2H bilayer $MoSe_2$. (c) Log-plot of SHG intensity from monolayer or 2H bilayer $MoSe_2$ under different strain amplitudes. The negligible SHG response in bilayer reveals the perfect transferring of strain from the bottom layer to the top layer.

DOI: 10.1021/acs.nanolett.7b03476
Nano Lett. 2017, 17, 7539−7543

To address this issue, we choose 2H $MoSe_2$ bilayers where the bottom layer is larger than the top layer (Figure 3b). The respective E^1_{2g}, A_{1g}, and C modes located at 241.8, 287.3, and 19.2 cm^{-1} confirm bilayer configuration (Figure 1b). The bottom layer of $MoSe_2$ is directly subject to uniaxial tensile strain $\varepsilon_{\text{bottom}}$ from the substrate as monitored by PL peak positions (Supplementary Figure S7). The 2H bilayer $MoSe_2$ belongs to the centrosymmetric D_{3d} point group, and the presence of inversion symmetry does not allow SHG response. If the two layers can be locked under relative interlayer strain, the whole system retains its centrosymmetric symmetry with negligible SHG response; otherwise, appreciable SHG signal can be generated. Figure 3c shows the SHG intensity from the 2H bilayer region and monolayer region under strain. The SHG intensity from monolayer changes rapidly, while the SHG intensity from bilayer keeps very low (comparable to our detection limit) even when the applied strain is as large as 1.4% at the bottom layer. It reveals that the two layers are locked under relative interlayer strain at least up to 1.4%.

To understand this interlayer locking effect in $MoSe_2$ bilayer under the relatively large interlayer strain, we performed first-principles calculations (see SI for details). We first obtain the energy barrier for interlayer sliding along zigzag direction from AB_1 to AB_3 stacking as shown in the insets of Figure 4a. The results show that the interlayer sliding must overcome an energy barrier of ∼50 meV/cell. It means that the sliding needs some additional energy if the two layers are not locked. But surely, if the two layers are locked, the strain energy will increase. The final configuration will be determined by the competition between interlayer interaction energy and total strain energy. We further calculated the total energy increase of the bilayer system with strain being applied to the bottom layer when the two layers are locked (blue squares) or sliding (red circles) in Figure 4b. We find that the locked bilayer is energetically favorable at small strains (<1.3%) and interlayer sliding is possible when the strain is larger than 1.3%. The trend is in nice agreement with our experiment although the quantitative strain threshold has small deviation as the theoretical value is dependent on the approximations in calculation of van der Waals interactions.[47] Our results confirm that interlayer interaction can efficiently transfer strain of a few percentages from the bottom layer to the top layer in 2H bilayer $MoSe_2$. Here we note that the edge of the top layer may add additional energy to the whole system, as previous studies showed that the edge might be curved.[48] However, as the top layer in our experiment is as large as 5 μm, the atomic number ratio of edge/area is as small as ∼0.4% and the contribution of the edge would be negligible.

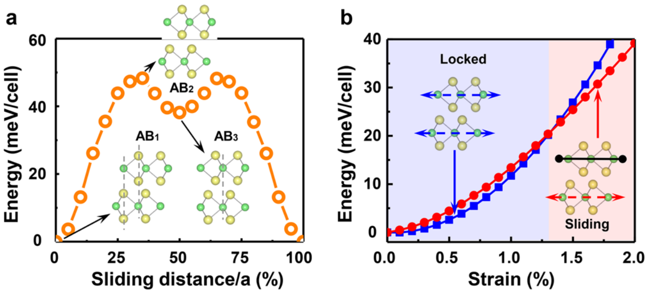

Figure 4. Theoretical understanding of the interlayer locking behavior in 2H $MoSe_2$ bilayer. (a) Potential energy of 2H $MoSe_2$ bilayer with interlayer sliding of one lattice constant along the zigzag direction. In horizontal axis, a is the lattice constant (3.33 Å) of $MoSe_2$. (b) Potential energy of 2H $MoSe_2$ bilayer under different strain amplitudes. "Locked" and "Sliding" represent the conditions that the strain is 100% or 0% transferred from the bottom layer to the top layer.

In summary, our work demonstrates the application of SHG to monitor the local strain vector in 2D $MoSe_2$ without in-plane mapping. The strain amplitude can be determined by the SHG intensity, while the strain direction can be indicated by the polarization-dependent SHG pattern evolution. In addition, we also utilize this technique to investigate the interlayer locking behavior in 2H $MoSe_2$ bilayers under relative interlayer strain. Our experimental results, together with ab initio calculations, show that the interlayer interactions can lock percentage level strain between the two layers in 2H $MoSe_2$ bilayer. SHG has limitation in characterizing centrosymmetric 2D system only, for example, in graphene there is no obvious SHG signal, but recent progress shows that even graphene can have high harmonic generation (HHG) signal.[49] If we use HHG, it is very promising to monitor the strain in any 2D materials in the near future.

■ ASSOCIATED CONTENT

Ⓢ Supporting Information

The Supporting Information is available free of charge on the ACS Publications website at DOI: 10.1021/acs.nanolett.7b03476.

Figures for strain dependence of PL peak position, SHG intensity, and PL peak energy mapping of monolayer $MoSe_2$, pattern evolution of SHG for monolayer $MoSe_2$ and MoS_2, evolution of normalized SHG intensity of monolayer MoS_2 with strain, strain response of tensor elements in $\overleftrightarrow{d}$ and PL spectrum of bilayer $MoSe_2$ under tensile strain. Notes for reduced symmetry of monolayer $MoSe_2$ under uniaxial strain. Table for parameters used to characterize strain-dependent $\overleftrightarrow{d}$. Detailed methods of synthesis and preparation of monolayer and bilayer $MoSe_2$, characterization of $MoSe_2$, SHG measurements, and theoretical calculations (PDF)

■ AUTHOR INFORMATION

Corresponding Authors

*E-mail: khliu@pku.edu.cn. Phone: +861062766013.
*E-mail: smeng@iphy.ac.cn. Phone: +861086249396.
*E-mail: zhipei.sun@aalto.fi. Phone: +358504302820.

ORCID

Jing Liang: 0000-0001-6348-2068
Jin Zhang: 0000-0001-7830-3464
Peng Gao: 0000-0003-0860-5525
Zhongfan Liu: 0000-0003-0065-7988
Zhipei Sun: 0000-0002-9771-5293
Sheng Meng: 0000-0002-1553-1432
Kaihui Liu: 0000-0002-8781-2495

Author Contributions

J.L., J.Z., Z. Li, and H.H. contributed equally to this work.

Notes

The authors declare no competing financial interest.

■ ACKNOWLEDGMENTS

We are grateful to Feng Wang (UC Berkeley) for the helpful comments. We thank Ding Pan (HongKong UST) for his help in revising the manuscript. This work was supported by the National Key R&D Program of China (2016YFA0300903, 2016YFA0300902, 2016YFA0300904), the National Natural Science Foundation of China (11474006, 51522201), and National Program for Thousand Young Talents of China.

■ REFERENCES

(1) Novoselov, K. S.; Jiang, D.; Schedin, F.; Booth, T. J.; Khotkevich, V. V.; Morozov, S. V.; Geim, A. K. *Proc. Natl. Acad. Sci. U. S. A.* **2005**, *102*, 10451−10453.
(2) Geim, A. K.; Novoselov, K. S. *Nat. Mater.* **2007**, *6*, 183−191.
(3) Splendiani, A.; Sun, L.; Zhang, Y. B.; Li, T. S.; Kim, J.; Chim, C. Y.; Galli, G.; Wang, F. *Nano Lett.* **2010**, *10*, 1271−1275.
(4) Mak, K. F.; Lee, C.; Hone, J.; Shan, J.; Heinz, T. F. *Phys. Rev. Lett.* **2010**, *105*, 136805.
(5) Wang, Q. H.; Kalantar-Zadeh, K.; Kis, A.; Coleman, J. N.; Strano, M. S. *Nat. Nanotechnol.* **2012**, *7*, 699−712.
(6) Du, Y. P.; Yin, Z. Y.; Zhu, J. X.; Huang, X.; Wu, X. J.; Zeng, Z. Y.; Yan, Q. Y.; Zhang, H. *Nat. Commun.* **2012**, *3*, 1177.
(7) Mak, K. F.; He, K. L.; Shan, J.; Heinz, T. F. *Nat. Nanotechnol.* **2012**, *7*, 494−498.
(8) Zeng, H. L.; Dai, J. F.; Yao, W.; Xiao, D.; Cui, X. D. *Nat. Nanotechnol.* **2012**, *7*, 490−493.
(9) Mak, K. F.; McGill, K. L.; Park, J.; McEuen, P. L. *Science* **2014**, *344*, 1489−1492.
(10) Li, L. K.; Yu, Y. J.; Ye, G. J.; Ge, Q. Q.; Ou, X. D.; Wu, H.; Feng, D. L.; Chen, X. H.; Zhang, Y. B. *Nat. Nanotechnol.* **2014**, *9*, 372−377.
(11) Dou, L. T.; Wong, A. B.; Yu, Y.; Lai, M. L.; Kornienko, N.; Eaton, S. W.; Fu, A.; Bischak, C. G.; Ma, J.; Ding, T. N.; Ginsberg, N. S.; Wang, L. W.; Alivisatos, A. P.; Yang, P. D. *Science* **2015**, *349*, 1518−1521.
(12) Wu, S.; Buckley, S.; Schaibley, J. R.; Feng, L.; Yan, J.; Mandrus, D. G.; Hatami, F.; Yao, W.; Vuckovic, J.; Majumdar, A.; Xu, X. *Nature* **2015**, *520*, 69−72.
(13) Ha, S. T.; Shen, C.; Zhang, J.; Xiong, Q. H. *Nat. Photonics* **2016**, *10*, 115−121.
(14) Tran, T. T.; Bray, K.; Ford, M. J.; Toth, M.; Aharonovich, I. *Nat. Nanotechnol.* **2016**, *11*, 37−41.
(15) Avouris, P.; Heinz, T. F.; Low, T. *2D Materials: Properties and Devices*; Cambridge University Press, 2017.
(16) Lee, C.; Wei, X. D.; Kysar, J. W.; Hone, J. *Science* **2008**, *321*, 385−388.
(17) Bertolazzi, S.; Brivio, J.; Kis, A. *ACS Nano* **2011**, *5*, 9703−9709.
(18) Feng, J.; Qian, X.; Huang, C.-W.; Li, J. *Nat. Photonics* **2012**, *6*, 866−872.
(19) Hui, Y. Y.; Liu, X.; Jie, W.; Chan, N. Y.; Hao, J.; Hsu, Y. T.; Li, L. J.; Guo, W.; Lau, S. P. *ACS Nano* **2013**, *7*, 7126−7131.
(20) He, K.; Poole, C.; Mak, K. F.; Shan, J. *Nano Lett.* **2013**, *13*, 2931−2936.
(21) Conley, H. J.; Wang, B.; Ziegler, J. I.; Haglund, R. F., Jr.; Pantelides, S. T.; Bolotin, K. I. *Nano Lett.* **2013**, *13*, 3626−3630.
(22) Liu, Z.; Amani, M.; Najmaei, S.; Xu, Q.; Zou, X. L.; Zhou, W.; Yu, T.; Qiu, C. Y.; Birdwell, A. G.; Crowne, F. J.; Vajtai, R.; Yakobson, B. I.; Xia, Z. H.; Dubey, M.; Ajayan, P. M.; Lou, J. *Nat. Commun.* **2014**, *5*, 5246.
(23) Island, J. O.; Kuc, A.; Diependaal, E. H.; Bratschitsch, R.; van der Zant, H. S. J.; Heine, T.; Castellanos-Gomez, A. *Nanoscale* **2016**, *8*, 2589−2593.
(24) Hytch, M.; Houdellier, F.; Hue, F.; Snoeck, E. *Nature* **2008**, *453*, 1086−1089.
(25) Oguro, H.; Awaji, S.; Nishijima, G.; Takahashi, K.; Watanabe, K.; Machiya, S.; Suzuki, H.; Tsuchiya, Y.; Osamura, K. *Supercond. Sci. Technol.* **2010**, *23*, 24.
(26) Cassidy, D. T.; Lam, S. K.; Lakshmi, B.; Bruce, D. M. *Appl. Opt.* **2004**, *43*, 1811−1818.
(27) Huang, M. Y.; Yan, H. G.; Heinz, T. F.; Hone, J. *Nano Lett.* **2010**, *10*, 4074−4079.
(28) Huang, M. Y.; Yan, H. G.; Chen, C. Y.; Song, D. H.; Heinz, T. F.; Hone, J. *Proc. Natl. Acad. Sci. U. S. A.* **2009**, *106*, 7304−7308.
(29) Mohiuddin, T. M. G.; Lombardo, A.; Nair, R. R.; Bonetti, A.; Savini, G.; Jalil, R.; Bonini, N.; Basko, D. M.; Galiotis, C.; Marzari, N.; Novoselov, K. S.; Geim, A. K.; Ferrari, A. C. *Phys. Rev. B: Condens. Matter Mater. Phys.* **2009**, *79*, 205433.
(30) Wang, Y. L.; Cong, C. X.; Qiu, C. Y.; Yu, T. *Small* **2013**, *9*, 2857−2861.
(31) Li, Y. L.; Rao, Y.; Mak, K. F.; You, Y. M.; Wang, S. Y.; Dean, C. R.; Heinz, T. F. *Nano Lett.* **2013**, *13*, 3329−3333.
(32) Hsu, W. T.; Zhao, Z. A.; Li, L. J.; Chen, C. H.; Chiu, M. H.; Chang, P. S.; Chou, Y. C.; Chang, W. H. *ACS Nano* **2014**, *8*, 2951−2958.
(33) Yin, X. B.; Ye, Z. L.; Chenet, D. A.; Ye, Y.; O'Brien, K.; Hone, J. C.; Zhang, X. *Science* **2014**, *344*, 488−490.
(34) Cheng, J. X.; Jiang, T.; Ji, Q. Q.; Zhang, Y.; Li, Z. M.; Shan, Y. W.; Zhang, Y. F.; Gong, X. G.; Liu, W. T.; Wu, S. W. *Adv. Mater.* **2015**, *27*, 4069−4074.
(35) Zhou, X.; Cheng, J. X.; Zhou, Y. B.; Cao, T.; Hong, H.; Liao, Z. M.; Wu, S. W.; Peng, H. L.; Liu, K. H.; Yu, D. P. *J. Am. Chem. Soc.* **2015**, *137*, 7994−7997.
(36) Rhim, S. H.; Kim, Y. S.; Freeman, A. J. *Appl. Phys. Lett.* **2015**, *107*, 241908.
(37) Zhao, M.; Ye, Z. L.; Suzuki, R.; Ye, Y.; Zhu, H. Y.; Xiao, J.; Wang, Y.; Iwasa, Y.; Zhang, X. *Light: Sci. Appl.* **2016**, *5*, e16131.
(38) Wang, H.; Qian, X. *Nano Lett.* **2017**, *17*, 5027.
(39) Karvonen, L.; Saynatjoki, A.; Huttunen, M. J.; Autere, A.; Amirsolaimani, B.; Li, S.; Norwood, R. A.; Peyghambarian, N.; Lipsanen, H.; Eda, G.; Kieu, K.; Sun, Z. P. *Nat. Commun.* **2017**, *8*, 15714.
(40) Zhang, X.; Han, W. P.; Wu, J. B.; Milana, S.; Lu, Y.; Li, Q. Q.; Ferrari, A. C.; Tan, P. H. *Phys. Rev. B: Condens. Matter Mater. Phys.* **2013**, *87*, 1504−1509.
(41) Lu, X.; Utama, M. I. B.; Lin, J. H.; Luo, X.; Zhao, Y. Y.; Zhang, J.; Pantelides, S. T.; Zhou, W.; Quek, S. Y.; Xiong, Q. H. *Adv. Mater.* **2015**, *27*, 4502−4508.
(42) Tancogne-Dejean, N.; Mucke, O. D.; Kartner, F. X.; Rubio, A. *Phys. Rev. Lett.* **2017**, *118*, 087403.
(43) Boyd, R. W. *Nonlinear Optics*, third ed; Academic Press, 2008.
(44) Oviedo, J. P.; Santosh, K. C.; Lu, N.; Wang, J. G.; Cho, K.; Wallace, R. M.; Kim, M. J. *ACS Nano* **2015**, *9*, 1543−1551.
(45) Kumar, H.; Dong, L.; Shenoy, V. B. *Sci. Rep.* **2016**, *6*, 21516.
(46) Li, H.; Wang, J.; Gao, S.; Chen, Q.; Peng, L.; Liu, K.; Wei, X. *Adv. Mater.* **2017**, *29*, 1701474.
(47) Kresse, G.; Furthmuller, J. *Phys. Rev. B: Condens. Matter Mater. Phys.* **1996**, *54*, 11169−11186.
(48) Tao, C. G.; Jiao, L. Y.; Yazyev, O. V.; Chen, Y. C.; Feng, J. J.; Zhang, X. W.; Capaz, R. B.; Tour, J. M.; Zettl, A.; Louie, S. G.; Dai, H. J.; Crommie, M. F. *Nat. Phys.* **2011**, *7*, 616−620.
(49) Yoshikawa, N.; Tamaya, T.; Tanaka, K. *Science* **2017**, *356*, 736−738.

DOI: 10.1021/acs.nanolett.7b03476
Nano Lett. 2017, 17, 7539−7543